

First Observation of the Rare Purely Baryonic Decay $B^0 \rightarrow p\bar{p}$

R. Aaij *et al.*^{*}

(LHCb Collaboration)

(Received 7 September 2017; published 4 December 2017)

The first observation of the decay of a B^0 meson to a purely baryonic final state, $B^0 \rightarrow p\bar{p}$, is reported. The proton-proton collision data sample used was collected with the LHCb experiment at center-of-mass energies of 7 and 8 TeV and corresponds to an integrated luminosity of 3.0 fb^{-1} . The branching fraction is determined to be $\mathcal{B}(B^0 \rightarrow p\bar{p}) = (1.25 \pm 0.27 \pm 0.18) \times 10^{-8}$, where the first uncertainty is statistical and the second systematic. The decay mode $B^0 \rightarrow p\bar{p}$ is the rarest decay of the B^0 meson observed to date. The decay $B_s^0 \rightarrow p\bar{p}$ is also investigated. No signal is seen and the upper limit $\mathcal{B}(B_s^0 \rightarrow p\bar{p}) < 1.5 \times 10^{-8}$ at 90% confidence level is set on the branching fraction.

DOI: 10.1103/PhysRevLett.119.232001

Studies of B mesons decaying to baryonic final states have been carried out since the late 1990s [1]. It was quickly realized that baryonic and mesonic B -meson decays differ in a number of ways. Two-body baryonic decays are suppressed with respect to decays to multibody final states [2,3] and the characteristic threshold enhancement in the baryon-antibaryon mass spectrum [4,5] is still not fully understood. The study of such decays provides information on the dynamics of B decays and tests QCD-based models of the hadronization process [5]. It helps to discriminate the available models and makes it possible to extract both tree and penguin amplitudes of charmless two-body baryonic decays when combining the information on the $B^0 \rightarrow p\bar{p}$ and $B^+ \rightarrow p\bar{\Lambda}$ branching fractions [6].

Baryonic B decays are also interesting in the study of CP violation. First evidence of CP violation in baryonic B decays has been reported from the analysis of $B^+ \rightarrow p\bar{p}K^+$ decays [7] and awaits confirmation in other decay modes [8].

This Letter presents a search for the suppressed decays of B^0 and B_s^0 mesons to the two-body charmless baryonic final state $p\bar{p}$. Prior to searches at the LHC, the ALEPH, CLEO, BABAR, and Belle Collaborations searched for the $B^0 \rightarrow p\bar{p}$ decay [9–12]. The most stringent upper limit on its branching fraction was obtained by the Belle experiment and is $\mathcal{B}(B^0 \rightarrow p\bar{p}) < 1.1 \times 10^{-7}$ at 90% confidence level (C.L.) [12]. The only search for the $B_s^0 \rightarrow p\bar{p}$ decay, performed by the ALEPH Collaboration, yielded the upper limit $\mathcal{B}(B_s^0 \rightarrow p\bar{p}) < 5.9 \times 10^{-5}$ at 90% C.L. [9].

The LHCb Collaboration has greatly increased the knowledge of baryonic B decays in recent years [7,13–17]. The

collaboration has reported the first observation of a two-body charmless baryonic B^+ decay, $B^+ \rightarrow p\bar{\Lambda}(1520)$ [7], and the first evidence for $B^0 \rightarrow p\bar{p}$, a two-body charmless baryonic decay of the B^0 meson [13]. The experimental data on two-body final states is nevertheless scarce. The study of these suppressed modes requires large data samples that are presently only available at the LHC.

In this analysis, in order to suppress common systematic uncertainties, the branching fractions of the $B^0 \rightarrow p\bar{p}$ and $B_s^0 \rightarrow p\bar{p}$ decays are measured using the topologically identical decay $B^0 \rightarrow K^+\pi^-$. The branching fractions are determined from

$$\mathcal{B}(B_{(s)}^0 \rightarrow p\bar{p}) = \frac{N(B_{(s)}^0 \rightarrow p\bar{p})}{N(B^0 \rightarrow K^+\pi^-)} \frac{\epsilon_{B^0 \rightarrow K^+\pi^-}}{\epsilon_{B_{(s)}^0 \rightarrow p\bar{p}}} \times \mathcal{B}(B^0 \rightarrow K^+\pi^-) \left(\times \frac{f_d}{f_s} \right), \quad (1)$$

where N represents yields determined from fits to the $p\bar{p}$ or $K^+\pi^-$ invariant-mass distributions, f_d/f_s (included only for the B_s^0 mode) is the ratio of b -quark hadronization probabilities into the B^0 and B_s^0 mesons [18] and ϵ represents the geometrical acceptance, reconstruction, and selection efficiencies. The notation $B_{(s)}^0 \rightarrow p\bar{p}$ stands for either $B^0 \rightarrow p\bar{p}$ or $B_s^0 \rightarrow p\bar{p}$. The inclusion of charge-conjugate processes is implied, unless otherwise indicated.

The data sample analyzed corresponds to an integrated luminosity of 1.0 fb^{-1} of proton-proton collision data collected by the LHCb experiment at center-of-mass energies of 7 TeV in 2011 and 2.0 fb^{-1} at 8 TeV in 2012. The LHCb detector [19,20] is a single-arm forward spectrometer covering the pseudorapidity range $2 < \eta < 5$, designed for the study of particles containing b or c quarks. The detector includes a high-precision tracking system consisting of a silicon-strip vertex detector surrounding the pp interaction region [21], a large-area silicon-strip

*Full author list given at the end of the article.

Published by the American Physical Society under the terms of the Creative Commons Attribution 4.0 International license. Further distribution of this work must maintain attribution to the author(s) and the published article's title, journal citation, and DOI.

detector located upstream of a dipole magnet with a bending power of about 4 Tm, and three stations of silicon-strip detectors and straw drift tubes [22] placed downstream of the magnet. The tracking system provides a measurement of momentum p of charged particles with a relative uncertainty that varies from 0.5% at low momentum to 1.0% at 200 GeV/c. The minimum distance of a track to a primary vertex (PV), the impact parameter (IP), is measured with a resolution of $(15 + 29/p_T) \mu\text{m}$, where p_T is the component of the momentum transverse to the beam, in GeV/c. Different types of charged hadrons are distinguished using information from two ring-imaging Cherenkov detectors [23]. Photons, electrons, and hadrons are identified by a calorimeter system consisting of scintillating-pad and preshower detectors, an electromagnetic calorimeter, and a hadronic calorimeter. Muons are identified by a system composed of alternating layers of iron and detector planes consisting of multiwire proportional chambers and gas electron multipliers. Simulated data samples, produced as described in Refs. [24–29], are used to evaluate the response of the detector and to investigate and characterize possible sources of background.

Candidates are selected in a similar way for both signal $B_{(s)}^0 \rightarrow p\bar{p}$ decays and the normalization channel $B^0 \rightarrow K^+\pi^-$. Real-time event selection is performed by a trigger [30] consisting of a hardware stage, based on information from the calorimeter and muon systems, followed by a software stage, which performs a full event reconstruction. The hardware trigger stage requires events to have a hadron, photon, or electron with high transverse energy (above a few GeV) deposited in the calorimeters, or a muon with high transverse momentum. For this analysis, the hardware trigger decision can be made either on the signal candidates or on other particles in the event. The software trigger requires a two-track secondary vertex with a significant displacement from the PVs. At least one charged particle must have high p_T and be inconsistent with originating from a PV. A multivariate algorithm [31] is used for the identification of secondary vertices consistent with the decay of a b or c hadron.

The final selection of candidates in the signal and normalization modes is carried out with a preselection stage, particle identification (PID) criteria, and a requirement on the response of a multilayer perceptron (MLP) classifier [32]. To avoid potential biases, $p\bar{p}$ candidates with invariant mass in the range [5230, 5417] MeV/c² (± 50 MeV/c² window approximately three times the invariant-mass resolution around the known B^0 and B_s^0 masses [33]) were not examined until the analysis procedure was finalized.

At the preselection stage, the $B_{(s)}^0$ decay products are associated with tracks with good reconstruction quality that have $\chi_{\text{IP}}^2 > 9$ with respect to any PV, where the χ_{IP}^2 is defined as the difference between the vertex-fit χ^2 of a PV reconstructed with and without the track in question. The

minimum p_T of the decay products is required to be above 900 MeV/c and at least one of the decay products is required to have $p_T > 2100$ MeV/c. A loose PID requirement, based primarily on information from the Cherenkov detectors, is also imposed on both particles. The $B_{(s)}^0$ candidate must have a vertex with good reconstruction quality, $p_T > 1000$ MeV/c and a $\chi_{\text{IP}}^2 < 36$ with respect to the associated PV. The associated PV is that with which it forms the smallest χ_{IP}^2 . The angle θ_B between the momentum vector of the $B_{(s)}^0$ candidate and the line connecting the associated PV and the candidate's decay vertex is required to be close to zero [$\cos(\theta_B) > 0.9995$].

After preselection, tight PID requirements are applied to the two final-state particles to suppress so-called combinatorial background formed from the accidental associations of tracks unrelated to the signal decays, and to reduce contamination from b -hadron decays where one or more decay products are misidentified. The PID requirements are determined by optimizing the figure of merit $\epsilon^{\text{sig}}/(a/2 + \sqrt{N_{\text{bkg}}})$ [34], where $a = 5$ quantifies the target level of significance in standard deviations and ϵ^{sig} is the PID efficiency of the signal selection. The quantity N_{bkg} denotes the expected number of background events in the signal region. This is estimated by extrapolating the result of a fit to the invariant-mass distribution of the data in the sideband regions above and below the signal region. The PID criteria are allowed to be different for protons and antiprotons. The optimization of the PID criteria applied to the normalization decay candidates relies on maximizing the signal significance, while minimizing the contamination from misidentified backgrounds.

Further separation between signal and combinatorial background candidates relies on an MLP implemented with the TMVA toolkit [35]. There are ten input quantities to the MLP classifier: the minimum values of the p_T and η of the decay products, the scalar sum of their p_T values, the χ_{IP}^2 of the decay products; the distance of closest approach between the two decay products; a parameter expressing the quality of the $B_{(s)}^0$ vertex fit; the χ_{IP}^2 and θ_B angle of the $B_{(s)}^0$ candidate; and the p_T asymmetry within a cone around the $B_{(s)}^0$ direction defined by $A_{p_T} = (p_T^B - p_T^{\text{cone}})/(p_T^B + p_T^{\text{cone}})$, where p_T^{cone} is the transverse component of the vector sum of the momenta of all tracks measured within the cone radius $R = 1.0$ around the $B_{(s)}^0$ direction, except for the $B_{(s)}^0$ decay products. The cone radius is defined in pseudorapidity and azimuthal angle (η, ϕ) as $R = \sqrt{(\Delta\eta)^2 + (\Delta\phi)^2}$. The A_{p_T} requirement exploits the relative isolation of signal decay products as compared with background. The MLP is trained using simulated $B^0 \rightarrow p\bar{p}$ decays and data candidates in the $p\bar{p}$ invariant-mass sideband above 5417 MeV/c² to represent the background. The requirement on the MLP response is optimized using the same figure of merit as that used for the optimization of the PID selection. The MLP

selection keeps approximately 60% of the signal candidates, while suppressing combinatorial background by 2 orders of magnitude. The MLP applied to the normalization decay candidates is the same as that trained to select the $B_{(s)}^0 \rightarrow p\bar{p}$ signal candidates, with the requirement on the response chosen to maximize the $B^0 \rightarrow K^+\pi^-$ significance. A vanishingly small fraction of events contains a second candidate after all selection requirements are applied and all candidates are kept.

Large control data samples of kinematically identified pions, kaons, and protons originating from the decays $D^0 \rightarrow K^-\pi^+$, $\Lambda \rightarrow p\pi^-$, and $\Lambda_c^+ \rightarrow pK^-\pi^+$ are employed to determine the efficiency of the PID requirements [23]. All the other components of the selection efficiencies are determined from simulation. The agreement between data and simulation is verified comparing kinematic distributions from selected $B^0 \rightarrow K^+\pi^-$ decays. The distributions in data are obtained with the *sPlot* technique [36] with the B^0 candidate invariant mass used as the discriminating variable. The overall efficiencies of this analysis, including the trigger selection and the reconstruction, are of the order 10^{-3} .

Sources of noncombinatorial background to the $p\bar{p}$ spectrum are investigated using simulation samples. These sources include partially reconstructed backgrounds in which one or more particles from the decay of a b hadron are not associated with the signal candidate, or b -hadron decays where one or more decay products are misidentified. The sum of such backgrounds does not peak in the B^0 and B_s^0 signal regions but rather contributes a smooth $p\bar{p}$ mass spectrum, which is indistinguishable from the dominant combinatorial background.

The yields of the signal and normalization candidates are determined using unbinned maximum likelihood fits to the invariant-mass distributions. The $p\bar{p}$ invariant-mass distribution is described with three components, namely the $B^0 \rightarrow p\bar{p}$ and $B_s^0 \rightarrow p\bar{p}$ signals and combinatorial background. The $B_{(s)}^0 \rightarrow p\bar{p}$ signals are modeled with the sum of two Crystal Ball (CB) functions [37] describing the high- and low-mass asymmetric tails. The two components of each signal share the same peak and core width parameters. The core widths are fixed using $B_{(s)}^0 \rightarrow p\bar{p}$ simulated samples. A scaling factor is applied to account for differences in the resolution between data and simulation as determined from $B^0 \rightarrow K^+\pi^-$ candidates. The $B_s^0 \rightarrow p\bar{p}$ signal peak value is set relative to the $B^0 \rightarrow p\bar{p}$ signal peak value determined from the fit according to the B_s^0 - B^0 mass difference [33]. The tail parameters and the relative normalization of the CB functions are determined from simulation. The combinatorial background is described with a linear function, with the slope parameter allowed to vary in the fit.

The $p\bar{p}$ invariant-mass distribution is presented in Fig. 1 together with the result of the fit. The yields of

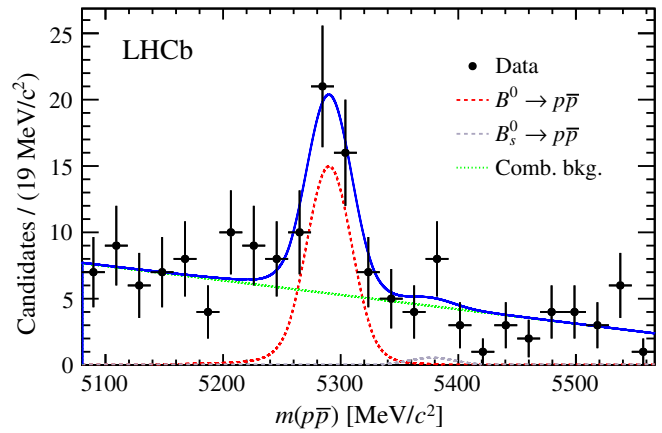


FIG. 1. Invariant mass distribution of $p\bar{p}$ candidates. The fit result (blue, solid line) is shown together with each fit model component: the $B^0 \rightarrow p\bar{p}$ signal (red, dashed line), the $B_s^0 \rightarrow p\bar{p}$ signal (gray, dashed line), and the combinatorial background (green, dotted line).

the $B_{(s)}^0 \rightarrow p\bar{p}$ signals are $N(B^0 \rightarrow p\bar{p}) = 39 \pm 8$ and $N(B_s^0 \rightarrow p\bar{p}) = 2 \pm 4$, where the uncertainties are statistical only. The significance of each of the signals is determined from the change in the logarithm of the likelihood between fits with and without the signal component [38]. The $B^0 \rightarrow p\bar{p}$ decay mode is found to have a significance of 5.3 standard deviations, including systematic uncertainties, and the $B_s^0 \rightarrow p\bar{p}$ mode is found to have a significance of 0.4 standard deviations, where, given its size, the significance has been evaluated ignoring systematic effects. The high significance of the $B^0 \rightarrow p\bar{p}$ signal implies the first observation of a two-body charmless baryonic B^0 decay.

The $K^+\pi^-$ invariant-mass distribution of the normalization decay candidates is described with components accounting for the $B^0 \rightarrow K^+\pi^-$ and $B_s^0 \rightarrow \pi^+K^-$ signals; the background due to the decays $B^0 \rightarrow \pi^+\pi^-$, $B_s^0 \rightarrow K^+K^-$, $\Lambda_b^0 \rightarrow p\pi^-$, and $\Lambda_b^0 \rightarrow pK^-$ when at least one of the final-state particles is misidentified; background from partially reconstructed b -hadron decays; and combinatorial background. The $B^0 \rightarrow K^+\pi^-$ and $B_s^0 \rightarrow \pi^+K^-$ decays are modeled with the sum of two CB functions sharing the same peak and core width parameters. The peak value and core width of the $B^0 \rightarrow K^+\pi^-$ signal model are free parameters in the fit. The difference between the peak positions of the $B^0 \rightarrow K^+\pi^-$ and $B_s^0 \rightarrow \pi^+K^-$ signals is constrained to its known value [33] and the core width of the $B_s^0 \rightarrow \pi^+K^-$ signal is related to the $B^0 \rightarrow K^+\pi^-$ signal core width by a scaling factor of 1.02 as determined from simulation. The tail parameters and the relative normalization of both double CB functions are determined from simulation. The invariant-mass distributions of the four misidentified decays are determined from simulation and are modeled with nonparametric functions [39]. The relative fractions of these background components

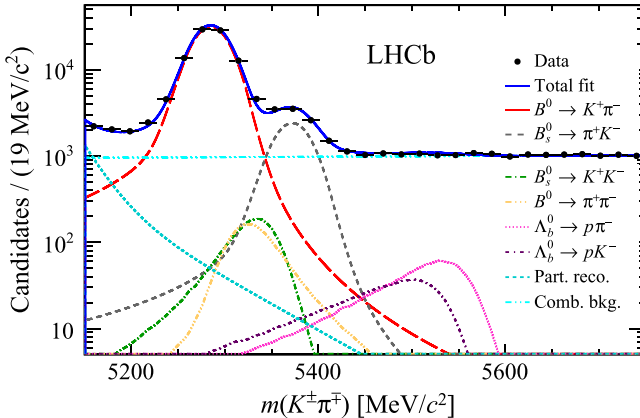


FIG. 2. Invariant mass distribution of $K^\pm\pi^\mp$ candidates. The fit result (blue, solid line) is shown together with each fit model component.

depend upon the branching fractions, b -hadron hadronization probabilities, and misidentification rates of the backgrounds. The fractions are Gaussian constrained to the product of these three factors, with the widths of the Gaussian functions equal to their combined uncertainties. The misidentification rates are determined from calibration data samples, whereas all other selection efficiencies are obtained from simulation. Partially reconstructed backgrounds represent decay modes misreconstructed as signal with one or more undetected final-state particles, possibly in conjunction with misidentifications. The shapes of these backgrounds in $K^\pm\pi^\mp$ invariant mass are determined from simulation, where each contributing decay is assigned a weight dependent on its relative branching fraction, hadronization probability, and selection efficiency. The weighted sum of the partially reconstructed backgrounds is well modeled with the sum of two exponential functions, the slope parameters of which are fixed from simulation, while the yield is determined in the fit to the data. As for the signal fit, the combinatorial background is described with a linear function, with the slope parameter allowed to vary in the fit.

The fit to the $K^\pm\pi^\mp$ invariant mass, shown in Fig. 2, involves seven fitted parameters and yields $N(B^0 \rightarrow K^\pm\pi^\mp) = 88961 \pm 341$ signal decays, where the uncertainty is statistical only.

The sources of systematic uncertainty on the $B_{(s)}^0 \rightarrow p\bar{p}$ branching fractions arise from the fit model, the limited knowledge of the selection efficiencies, and the uncertainties on the $B^0 \rightarrow K^\pm\pi^\mp$ branching fraction and on the ratio of b -quark hadronization probabilities f_s/f_d . Pseudoexperiments are used to estimate the effects of using alternative shapes for the fit components and of including additional backgrounds in the fit. Systematic uncertainties on the fit models are also assessed by varying the fixed parameters of the models within their uncertainties. The description of the combinatorial background is replaced by an exponential function. In the fit to the signal

modes, the partially reconstructed decays $B^+ \rightarrow p\bar{p}\ell^+\bar{\nu}_\ell$, where ℓ stands for an electron or a muon and ν_ℓ for the corresponding neutrino, are added to the fit model. Intrinsic biases in the fitted yields are also investigated with pseudoexperiments and are found to be negligible.

Uncertainties on the efficiencies arise from residual differences between data and simulation in the trigger, reconstruction, selection, and uncertainties on the data-driven particle identification efficiencies. These differences are assessed using the $B^0 \rightarrow K^+\pi^-$ normalization decay, comparing the level of agreement between simulation and data. The distributions of selection variables for $B^0 \rightarrow K^+\pi^-$ signal candidates in data are obtained by subtracting the background using the *sPlot* technique [36], with the $K^+\pi^-$ candidate invariant mass as the discriminating variable. The effect of binning the PID calibration samples used to obtain the PID efficiencies is evaluated by varying the binning scheme and by adding an extra dimension accounting for event multiplicity to the binning of the samples.

The uncertainty on the branching fraction of the normalization decay, $\mathcal{B}(B^0 \rightarrow K^+\pi^-) = (1.96 \pm 0.05) \times 10^{-5}$ [33], is taken as a systematic uncertainty from external inputs. The uncertainty on the measurement $f_s/f_d = 0.259 \pm 0.015$ [18] is quoted as a separate source of systematic uncertainty from external inputs in the determination of the upper limit on $\mathcal{B}(B_s^0 \rightarrow p\bar{p})$. The total systematic uncertainty on the $B^0 \rightarrow p\bar{p}$ ($B_s^0 \rightarrow p\bar{p}$) branching fraction is given by the sum of all uncertainties added in quadrature and amounts to 14.2% (209%). The systematic uncertainties on the $B^0 \rightarrow p\bar{p}$ ($B_s^0 \rightarrow p\bar{p}$) branching fraction are dominated by the uncertainties on the fit model, which are 7.3% (208%), and on the reconstruction and selection efficiencies, which amount to 6.1% (6.1%) and 8.6% (8.3%), respectively. Specifically, the systematic uncertainty arising from the description of the fit model backgrounds dominates the uncertainty on the $B_s^0 \rightarrow p\bar{p}$ branching fraction.

In summary, the first observation of the simplest decay of a B^0 meson to a purely baryonic final state, $B^0 \rightarrow p\bar{p}$, is reported using a data sample of proton-proton collisions collected with the LHCb experiment, corresponding to a total integrated luminosity of 3.0 fb^{-1} . This rare two-body charmless baryonic decay is observed with a significance of 5.3 standard deviations, including systematic uncertainties. The $B^0 \rightarrow p\bar{p}$ branching fraction is determined to be

$$\mathcal{B}(B^0 \rightarrow p\bar{p}) = (1.25 \pm 0.27 \pm 0.18) \times 10^{-8},$$

where the first uncertainty is statistical and the second systematic. Since no $B_s^0 \rightarrow p\bar{p}$ signal is seen, the world's best upper limit $\mathcal{B}(B_s^0 \rightarrow p\bar{p}) < 1.5 \times 10^{-8}$ at 90% confidence level is set on the decay branching fraction using the Feldman-Cousins frequentist method [40].

The first observation of the decay $B^0 \rightarrow p\bar{p}$, the rarest B^0 decay ever observed, provides valuable input towards the understanding of the dynamics of hadronic B decays.

This measurement helps to discriminate among several QCD-based models and makes it possible to extract both tree and penguin amplitudes of charmless two-body baryonic decays when combining the information on the $B^0 \rightarrow p\bar{p}$ and $B^+ \rightarrow p\bar{\Lambda}$ branching fractions [6]. The measured $B^0 \rightarrow p\bar{p}$ branching fraction is compatible with recent theoretical calculations, as is the upper limit on the $B_s^0 \rightarrow p\bar{p}$ branching fraction [2,3,6]. An improved measurement of the $B_s^0 \rightarrow p\bar{p}$ branching fraction will make it possible to quantitatively compare the models proposed in Refs. [2,6].

We express our gratitude to our colleagues in the CERN accelerator departments for the excellent performance of the LHC. We thank the technical and administrative staff at the LHCb institutes. We acknowledge support from CERN and from the national agencies: CAPES, CNPq, FAPERJ and FINEP (Brazil); MOST and NSFC (China); CNRS, IN2P3 (France); BMBF, DFG and MPG (Germany); INFN (Italy); NWO (The Netherlands); MNiSW and NCN (Poland); MEN/IFA (Romania); MinES and FASO (Russia); MinECo (Spain); SNSF and SER (Switzerland); NASU (Ukraine); STFC (United Kingdom); NSF (USA). We acknowledge the computing resources that are provided by CERN, IN2P3 (France), KIT and DESY (Germany), INFN (Italy), SURF (The Netherlands), PIC (Spain), GridPP (United Kingdom), RRCKI and Yandex LLC (Russia), CSCS (Switzerland), IFIN-HH (Romania), CBPF (Brazil), PL-GRID (Poland) and OSC (USA). We are indebted to the communities behind the multiple open-source software packages on which we depend. Individual groups or members have received support from AvH Foundation (Germany), EPLANET, Marie Skłodowska-Curie Actions and ERC (European Union), ANR, Labex P2IO, ENIGMASS and OCEVU, and Région Auvergne-Rhône-Alpes (France), RFBR and Yandex LLC (Russia), GVA, XuntaGal and GENCAT (Spain), Herchel Smith Fund, the Royal Society, the English-Speaking Union and the Leverhulme Trust (United Kingdom).

- [1] X. Fu *et al.* (CLEO Collaboration), Observation of Exclusive B Decays to Final States Containing a Charmed Baryon, *Phys. Rev. Lett.* **79**, 3125 (1997).
- [2] Y.-K. Hsiao and C. Q. Geng, Violation of partial conservation of the axial-vector current and two-body baryonic B and D_s decays, *Phys. Rev. D* **91**, 077501 (2015).
- [3] H.-Y. Cheng and C.-K. Chua, On the smallness of tree-dominated charmless two-body baryonic B decay rates, *Phys. Rev. D* **91**, 036003 (2015).
- [4] W.-S. Hou and A. Soni, Pathways to Rare Baryonic B Decays, *Phys. Rev. Lett.* **86**, 4247 (2001).
- [5] A. J. Bevan *et al.* (BABAR and Belle Collaborations), The physics of the B factories, *Eur. Phys. J. C* **74**, 3026 (2014).
- [6] C.-K. Chua, Rates and CP asymmetries of charmless two-body baryonic $B_{u,d,s}$ decays, *Phys. Rev. D* **95**, 096004 (2017).

- [7] R. Aaij *et al.* (LHCb Collaboration), Evidence for CP Violation in $B^+ \rightarrow p\bar{p}K^+$ Decays, *Phys. Rev. Lett.* **113**, 141801 (2014).
- [8] C. Q. Geng, Y. K. Hsiao, and J. N. Ng, Direct CP Violation in $B^\pm \rightarrow p\bar{p}K^{(*)\pm}$, *Phys. Rev. Lett.* **98**, 011801 (2007).
- [9] D. Buskulic *et al.* (ALEPH Collaboration), Observation of charmless hadronic B decays, *Phys. Lett. B* **384**, 471 (1996).
- [10] T. E. Coan *et al.* (CLEO Collaboration), Search for exclusive rare baryonic decays of B mesons, *Phys. Rev. D* **59**, 111101 (1999).
- [11] B. Aubert *et al.* (BABAR Collaboration), Search for the decay $B^0 \rightarrow p\bar{p}$, *Phys. Rev. D* **69**, 091503 (2004).
- [12] Y.-T. Tsai *et al.* (Belle Collaboration), Search for $B^0 \rightarrow p\bar{p}, \Lambda\bar{\Lambda}$ and $B^+ \rightarrow p\bar{\Lambda}$ at Belle, *Phys. Rev. D* **75**, 111101 (2007).
- [13] R. Aaij *et al.* (LHCb Collaboration), First evidence for the two-body charmless baryonic decay $B^0 \rightarrow p\bar{p}$, *J. High Energy Phys.* **10** (2013) 005.
- [14] R. Aaij *et al.* (LHCb Collaboration), First Observation of a Baryonic B_c^+ Decay, *Phys. Rev. Lett.* **113**, 152003 (2014).
- [15] R. Aaij *et al.* (LHCb Collaboration), Evidence for the two-body charmless baryonic decay $B^+ \rightarrow p\bar{\Lambda}$, *J. High Energy Phys.* **04** (2017) 162.
- [16] R. Aaij *et al.* (LHCb Collaboration), First Observation of a Baryonic B_s^0 Decay, *Phys. Rev. Lett.* **119**, 041802 (2017).
- [17] R. Aaij *et al.* (LHCb Collaboration), Observation of charmless baryonic decays $B_{(s)}^0 \rightarrow p\bar{p}h^+h^-$, *Phys. Rev. D* **96**, 051103 (2017).
- [18] R. Aaij *et al.* (LHCb Collaboration), Measurement of the fragmentation fraction ratio f_s/f_d and its dependence on B meson kinematics, *J. High Energy Phys.* **04** (2013) 001, f_s/f_d value updated in LHCb-CONF-2013-011.
- [19] A. A. Alves Jr. *et al.* (LHCb Collaboration), The LHCb detector at the LHC, *J. Instrum.* **3**, S08005 (2008).
- [20] R. Aaij *et al.* (LHCb Collaboration), LHCb detector performance, *Int. J. Mod. Phys. A* **30**, 1530022 (2015).
- [21] R. Aaij *et al.* (LHCb Collaboration), Performance of the LHCb Vertex Locator, *J. Instrum.* **9**, P09007 (2014).
- [22] R. Arink *et al.* (LHCb Collaboration), Performance of the LHCb Outer Tracker, *J. Instrum.* **9**, P01002 (2014).
- [23] M. Adinolfi *et al.*, Performance of the LHCb RICH detector at the LHC, *Eur. Phys. J. C* **73**, 2431 (2013).
- [24] T. Sjöstrand, S. Mrenna, and P. Skands, A brief introduction to PYTHIA 8.1, *Comput. Phys. Commun.* **178**, 852 (2008); T. Sjöstrand, S. Mrenna, and P. Skands, PYTHIA 6.4 physics and manual, *J. High Energy Phys.* **05** (2006) 026.
- [25] I. Belyaev *et al.*, Handling of the generation of primary events in Gauss, the LHCb simulation framework, *J. Phys. Conf. Ser.* **331**, 032047 (2011).
- [26] D. J. Lange, The EvtGen particle decay simulation package, *Nucl. Instrum. Methods Phys. Res., Sect. A* **462**, 152 (2001).
- [27] P. Golonka and Z. Was, PHOTOS Monte Carlo: A precision tool for QED corrections in Z and W decays, *Eur. Phys. J. C* **45**, 97 (2006).
- [28] J. Allison *et al.* (Geant4 Collaboration), Geant4 developments and applications, *IEEE Trans. Nucl. Sci.* **53**, 270 (2006); S. Agostinelli *et al.* (Geant4 Collaboration), Geant4: A simulation toolkit, *Nucl. Instrum. Methods Phys. Res., Sect. A* **506**, 250 (2003).

- [29] M. Clemencic, G. Corti, S. Easo, C. R. Jones, S. Miglioranzi, M. Pappagallo, and P. Robbe, The LHCb simulation application, Gauss: Design, evolution and experience, *J. Phys. Conf. Ser.* **331**, 032023 (2011).
- [30] R. Aaij *et al.*, The LHCb trigger and its performance in 2011, *J. Instrum.* **8**, P04022 (2013).
- [31] V. V. Gligorov and M. Williams, Efficient, reliable and fast high-level triggering using a bonsai boosted decision tree, *J. Instrum.* **8**, P02013 (2013).
- [32] D. E. Rumelhart, G. E. Hinton, and R. J. Williams, *Parallel distributed processing: explorations in the microstructure of cognition* (MIT, Cambridge, MA, 1986), Vol. 1.
- [33] C. Patrignani *et al.* (Particle Data Group Collaboration), Review of particle physics, *Chin. Phys. C* **40**, 100001 (2016).
- [34] G. Punzi, Sensitivity of searches for new signals and its optimization, in *Statistical Problems in Particle Physics, Astrophysics, and Cosmology*, edited by L. Lyons, R. Mount, and R. Reitmeyer, eConf C030908, 79 (2003), arXiv:physics/0308063.
- [35] P. Speckmayer, A. Hoecker, J. Stelzer, and H. Voss, The toolkit for multivariate data analysis: TMVA 4, *J. Phys. Conf. Ser.* **219**, 032057 (2010).
- [36] M. Pivk and F. R. Le Diberder, sPlot: A statistical tool to unfold data distributions, *Nucl. Instrum. Methods Phys. Res., Sect. A* **555**, 356 (2005).
- [37] T. Skwarnicki, Ph.D. thesis, Institute of Nuclear Physics, Krakow, 1986, DESY-F31-86-02.
- [38] S. S. Wilks, The large-sample distribution of the likelihood ratio for testing composite hypotheses, *Ann. Math. Stat.* **9**, 60 (1938).
- [39] K. S. Cranmer, Kernel estimation in high-energy physics, *Comput. Phys. Commun.* **136**, 198 (2001).
- [40] G. J. Feldman and R. D. Cousins, Unified approach to the classical statistical analysis of small signals, *Phys. Rev. D* **57**, 3873 (1998).

-
- R. Aaij,⁴⁰ B. Adeva,³⁹ M. Adinolfi,⁴⁸ Z. Ajaltouni,⁵ S. Akar,⁵⁹ J. Albrecht,¹⁰ F. Alessio,⁴⁰ M. Alexander,⁵³ A. Alfonso Albero,³⁸ S. Ali,⁴³ G. Alkhazov,³¹ P. Alvarez Cartelle,⁵⁵ A. A. Alves Jr.,⁵⁹ S. Amato,² S. Amerio,²³ Y. Amhis,⁷ L. An,³ L. Anderlini,¹⁸ G. Andreassi,⁴¹ M. Andreotti,^{17,a} J. E. Andrews,⁶⁰ R. B. Appleby,⁵⁶ F. Archilli,⁴³ P. d'Argent,¹² J. Arnau Romeu,⁶ A. Artamonov,³⁷ M. Artuso,⁶¹ E. Aslanides,⁶ G. Auriemma,²⁶ M. Baalouch,⁵ I. Babuschkin,⁵⁶ S. Bachmann,¹² J. J. Back,⁵⁰ A. Badalov,^{38,b} C. Baesso,⁶² S. Baker,⁵⁵ V. Balagura,^{7,c} W. Baldini,¹⁷ A. Baranov,³⁵ R. J. Barlow,⁵⁶ C. Barschel,⁴⁰ S. Barsuk,⁷ W. Barter,⁵⁶ F. Baryshnikov,³² V. Batozskaya,²⁹ V. Battista,⁴¹ A. Bay,⁴¹ L. Beaucourt,⁴ J. Beddow,⁵³ F. Bedeschi,²⁴ I. Bediaga,¹ A. Beiter,⁶¹ L. J. Bel,⁴³ N. Belyi,⁶³ V. Bellee,⁴¹ N. Belloli,^{21,d} K. Belous,³⁷ I. Belyaev,³² E. Ben-Haim,⁸ G. Bencivenni,¹⁹ S. Benson,⁴³ S. Beranek,⁹ A. Berezhnoy,³³ R. Bernet,⁴² D. Berninghoff,¹² E. Bertholet,⁸ A. Bertolin,²³ C. Betancourt,⁴² F. Betti,¹⁵ M.-O. Bettler,⁴⁰ M. van Beuzekom,⁴³ Ia. Bezshyiko,⁴² S. Bifani,⁴⁷ P. Billoir,⁸ A. Birnkraut,¹⁰ A. Bitadze,⁵⁶ A. Bizzeti,^{18,e} M. Bjørn,⁵⁷ T. Blake,⁵⁰ F. Blanc,⁴¹ J. Blouw,^{11,f} S. Blusk,⁶¹ V. Bocci,²⁶ T. Boettcher,⁵⁸ A. Bondar,^{36,f} N. Bondar,³¹ W. Bonivento,¹⁶ I. Bordyuzhin,³² A. Borgheresi,^{21,d} S. Borghi,⁵⁶ M. Borisjak,³⁵ M. Borsato,³⁹ F. Bossu,⁷ M. Boubdir,⁹ T. J. V. Bowcock,⁵⁴ E. Bowen,⁴² C. Bozzi,^{17,40} S. Braun,¹² T. Britton,⁶¹ J. Brodzicka,²⁷ D. Brundu,¹⁶ E. Buchanan,⁴⁸ C. Burr,⁵⁶ A. Bursche,^{16,g} J. Buytaert,⁴⁰ W. Byczynski,⁴⁰ S. Cadeddu,¹⁶ H. Cai,⁶⁴ R. Calabrese,^{17,a} R. Calladine,⁴⁷ M. Calvi,^{21,d} M. Calvo Gomez,^{38,b} A. Camboni,^{38,b} P. Campana,¹⁹ D. H. Campora Perez,⁴⁰ L. Capriotti,⁵⁶ A. Carbone,^{15,h} G. Carboni,^{25,i} R. Cardinale,^{20,j} A. Cardini,¹⁶ P. Carniti,^{21,d} L. Carson,⁵² K. Carvalho Akiba,² G. Casse,⁵⁴ L. Cassina,²¹ L. Castillo Garcia,⁴¹ M. Cattaneo,⁴⁰ G. Cavallero,^{20,40,j} R. Cenci,^{24,k} D. Chamont,⁷ M. Charles,⁸ Ph. Charpentier,⁴⁰ G. Chatzikonstantidis,⁴⁷ M. Chefdeville,⁴ S. Chen,⁵⁶ S. F. Cheung,⁵⁷ S.-G. Chitic,⁴⁰ V. Chobanova,³⁹ M. Chrzaszcz,^{42,27} A. Chubykin,³¹ P. Ciambrone,¹⁹ X. Cid Vidal,³⁹ G. Ciezarek,⁴³ P. E. L. Clarke,⁵² M. Clemencic,⁴⁰ H. V. Cliff,⁴⁹ J. Closier,⁴⁰ J. Cogan,⁶ E. Cogneras,⁵ V. Cogoni,^{16,g} L. Cojocariu,³⁰ P. Collins,⁴⁰ T. Colombo,⁴⁰ A. Comerma-Montells,¹² A. Contu,⁴⁰ A. Cook,⁴⁸ G. Coombs,⁴⁰ S. Coquereau,³⁸ G. Corti,⁴⁰ M. Corvo,^{17,a} C. M. Costa Sobral,⁵⁰ B. Couturier,⁴⁰ G. A. Cowan,⁵² D. C. Craik,⁵⁸ A. Crocombe,⁵⁰ M. Cruz Torres,¹ R. Currie,⁵² C. D'Ambrosio,⁴⁰ F. Da Cunha Marinho,² E. Dall'Occo,⁴³ J. Dalseno,⁴⁸ A. Davis,³ O. De Aguiar Francisco,⁵⁴ S. De Capua,⁵⁶ M. De Cian,¹² J. M. De Miranda,¹ L. De Paula,² M. De Serio,^{14,l} P. De Simone,¹⁹ C. T. Dean,⁵³ D. Decamp,⁴ L. Del Buono,⁸ H.-P. Dembinski,¹¹ M. Demmer,¹⁰ A. Dendek,²⁸ D. Derkach,³⁵ O. Deschamps,⁵ F. Dettori,⁵⁴ B. Dey,⁶⁵ A. Di Canto,⁴⁰ P. Di Nezza,¹⁹ H. Dijkstra,⁴⁰ F. Dordei,⁴⁰ M. Dorigo,⁴⁰ A. Dosil Suárez,³⁹ L. Douglas,⁵³ A. Dovbnya,⁴⁵ K. Dreimanis,⁵⁴ L. Dufour,⁴³ G. Dujany,⁸ P. Durante,⁴⁰ R. Dzhelyadin,³⁷ M. Dziewiecki,¹² A. Dziurda,⁴⁰ A. Dzyuba,³¹ S. Easo,⁵¹ M. Ebert,⁵² U. Egede,⁵⁵ V. Egorychev,³² S. Eidelman,^{36,f} S. Eisenhardt,⁵² U. Eitschberger,¹⁰ R. Ekelhof,¹⁰ L. Eklund,⁵³ S. Ely,⁶¹ S. Esen,¹² H. M. Evans,⁴⁹ T. Evans,⁵⁷ A. Falabella,¹⁵ N. Farley,⁴⁷ S. Farry,⁵⁴ D. Fazzini,^{21,d} L. Federici,²⁵ D. Ferguson,⁵² G. Fernandez,³⁸ P. Fernandez Declara,⁴⁰ A. Fernandez Prieto,³⁹ F. Ferrari,¹⁵ F. Ferreira Rodrigues,² M. Ferro-Luzzi,⁴⁰ S. Filippov,³⁴ R. A. Fini,¹⁴ M. Fiore,^{17,a} M. Fiorini,^{17,a} M. Firlej,²⁸ C. Fitzpatrick,⁴¹ T. Fiutowski,²⁸ F. Fleuret,^{7,c} K. Fohl,⁴⁰ M. Fontana,^{16,40} F. Fontanelli,^{20,j}

- D. C. Forshaw,⁶¹ R. Forty,⁴⁰ V. Franco Lima,⁵⁴ M. Frank,⁴⁰ C. Frei,⁴⁰ J. Fu,^{22,m} W. Funk,⁴⁰ E. Furfaro,^{25,i} C. Färber,⁴⁰ E. Gabriel,⁵² A. Gallas Torreira,³⁹ D. Galli,^{15,h} S. Gallorini,²³ S. Gambetta,⁵² M. Gandelman,² P. Gandini,⁵⁷ Y. Gao,³ L. M. Garcia Martin,⁷⁰ J. García Pardiñas,³⁹ J. Garra Tico,⁴⁹ L. Garrido,³⁸ P. J. Garsed,⁴⁹ D. Gascon,³⁸ C. Gaspar,⁴⁰ L. Gavardi,¹⁰ G. Gazzoni,⁵ D. Gerick,¹² E. Gersabeck,¹² M. Gersabeck,⁵⁶ T. Gershon,⁵⁰ Ph. Ghez,⁴ S. Giani,⁴¹ V. Gibson,⁴⁹ O. G. Girard,⁴¹ L. Giubega,³⁰ K. Gizzdov,⁵² V. V. Gligorov,⁸ D. Golubkov,³² A. Golutvin,^{55,40} A. Gomes,^{1,n} I. V. Gorelov,³³ C. Gotti,^{21,d} E. Govorkova,⁴³ J. P. Grabowski,¹² R. Graciani Diaz,³⁸ L. A. Granado Cardoso,⁴⁰ E. Graugés,³⁸ E. Graverini,⁴² G. Graziani,¹⁸ A. Grecu,³⁰ R. Greim,⁹ P. Griffith,¹⁶ L. Grillo,^{21,40,d} L. Gruber,⁴⁰ B. R. Gruberg Cazon,⁵⁷ O. Grünberg,⁶⁷ E. Gushchin,³⁴ Yu. Guz,³⁷ T. Gys,⁴⁰ C. Göbel,⁶² T. Hadavizadeh,⁵⁷ C. Hadjivasilou,⁵ G. Haefeli,⁴¹ C. Haen,⁴⁰ S. C. Haines,⁴⁹ B. Hamilton,⁶⁰ X. Han,¹² T. H. Hancock,⁵⁷ S. Hansmann-Menzemer,¹² N. Harnew,⁵⁷ S. T. Harnew,⁴⁸ J. Harrison,⁵⁶ C. Hasse,⁴⁰ M. Hatch,⁴⁰ J. He,⁶³ M. Hecker,⁵⁵ K. Heinicke,¹⁰ A. Heister,⁹ K. Hennessy,⁵⁴ P. Henrard,⁵ L. Henry,⁷⁰ E. van Herwijnen,⁴⁰ M. Heß,⁶⁷ A. Hicheur,² D. Hill,⁵⁷ C. Hombach,⁵⁶ P. H. Hopchev,⁴¹ Z. C. Huard,⁵⁹ W. Hulsbergen,⁴³ T. Humair,⁵⁵ M. Hushchyn,³⁵ D. Hutchcroft,⁵⁴ P. Ibis,¹⁰ M. Idzik,²⁸ P. Ilten,⁵⁸ R. Jacobsson,⁴⁰ J. Jalocha,⁵⁷ E. Jans,⁴³ A. Jawahery,⁶⁰ F. Jiang,³ M. John,⁵⁷ D. Johnson,⁴⁰ C. R. Jones,⁴⁹ C. Joram,⁴⁰ B. Jost,⁴⁰ N. Jurik,⁵⁷ S. Kandybei,⁴⁵ M. Karacson,⁴⁰ J. M. Kariuki,⁴⁸ S. Karodia,⁵³ N. Kazeev,³⁵ M. Kecke,¹² M. Kelsey,⁶¹ M. Kenzie,⁴⁹ T. Ketel,⁴⁴ E. Khairullin,³⁵ B. Khanji,¹² C. Khurewathanakul,⁴¹ T. Kirn,⁹ S. Klaver,⁵⁶ K. Klimaszewski,²⁹ T. Klimkovich,¹¹ S. Koliev,⁴⁶ M. Kolpin,¹² I. Komarov,⁴¹ R. Kopecna,¹² P. Koppenburg,⁴³ A. Kosmyntseva,³² S. Kotriakhova,³¹ M. Kozeiha,⁵ L. Kravchuk,³⁴ M. Kreps,⁵⁰ P. Krokovny,^{36,f} F. Kruse,¹⁰ W. Krzemien,²⁹ W. Kucewicz,^{27,o} M. Kucharczyk,²⁷ V. Kudryavtsev,^{36,f} A. K. Kuonen,⁴¹ K. Kurek,²⁹ T. Kvaratskheliya,^{32,40} D. Lacarrere,⁴⁰ G. Lafferty,⁵⁶ A. Lai,¹⁶ G. Lanfranchi,¹⁹ C. Langenbruch,⁹ T. Latham,⁵⁰ C. Lazzeroni,⁴⁷ R. Le Gac,⁶ A. Leflat,^{33,40} J. Lefrançois,⁷ R. Lefèvre,⁵ F. Lemaitre,⁴⁰ E. Lemos Cid,³⁹ O. Leroy,⁶ T. Lesiak,²⁷ B. Leverington,¹² P.-R. Li,⁶³ T. Li,³ Y. Li,⁷ Z. Li,⁶¹ T. Likhomanenko,⁶⁸ R. Lindner,⁴⁰ F. Lionetto,⁴² V. Lisovskyi,⁷ X. Liu,³ D. Loh,⁵⁰ A. Loi,¹⁶ I. Longstaff,⁵³ J. H. Lopes,² D. Lucchesi,^{23,p} M. Lucio Martinez,³⁹ H. Luo,⁵² A. Lupato,²³ E. Luppi,^{17,a} O. Lupton,⁴⁰ A. Lusiani,²⁴ X. Lyu,⁶³ F. Machefert,⁷ F. Maciuc,³⁰ V. Macko,⁴¹ P. Mackowiak,¹⁰ S. Maddrell-Mander,⁴⁸ O. Maev,^{31,40} K. Maguire,⁵⁶ D. Maisuzenko,³¹ M. W. Majewski,²⁸ S. Malde,⁵⁷ A. Malinin,⁶⁸ T. Maltsev,^{36,f} G. Manca,^{16,g} G. Mancinelli,⁶ P. Manning,⁶¹ D. Marangotto,^{22,m} J. Maratas,^{5,q} J. F. Marchand,⁴ U. Marconi,¹⁵ C. Marin Benito,³⁸ M. Marinangeli,⁴¹ P. Marino,⁴¹ J. Marks,¹² G. Martellotti,²⁶ M. Martin,⁶ M. Martinelli,⁴¹ D. Martinez Santos,³⁹ F. Martinez Vidal,⁷⁰ D. Martins Tostes,² L. M. Massacrier,⁷ A. Massafferri,¹ R. Matev,⁴⁰ A. Mathad,⁵⁰ Z. Mathe,⁴⁰ C. Matteuzzi,²¹ A. Mauri,⁴² E. Maurice,^{7,c} B. Maurin,⁴¹ A. Mazurov,⁴⁷ M. McCann,^{55,40} A. McNab,⁵⁶ R. McNulty,¹³ J. V. Mead,⁵⁴ B. Meadows,⁵⁹ C. Meaux,⁶ F. Meier,¹⁰ N. Meinert,⁶⁷ D. Melnychuk,²⁹ M. Merk,⁴³ A. Merli,^{22,40,m} E. Michielin,²³ D. A. Milanes,⁶⁶ E. Millard,⁵⁰ M.-N. Minard,⁴ L. Minzoni,¹⁷ D. S. Mitzel,¹² A. Mogini,⁸ J. Molina Rodriguez,¹ T. Mombacher,¹⁰ I. A. Monroy,⁶⁶ S. Monteil,⁵ M. Morandin,²³ M. J. Morello,^{24,k} O. Morgunova,⁶⁸ J. Moron,²⁸ A. B. Morris,⁵² R. Mountain,⁶¹ F. Muheim,⁵² M. Mulder,⁴³ D. Müller,⁵⁶ J. Müller,¹⁰ K. Müller,⁴² V. Müller,¹⁰ P. Naik,⁴⁸ T. Nakada,⁴¹ R. Nandakumar,⁵¹ A. Nandi,⁵⁷ I. Nasteva,² M. Needham,⁵² N. Neri,^{22,40} S. Neubert,¹² N. Neufeld,⁴⁰ M. Neuner,¹² T. D. Nguyen,⁴¹ C. Nguyen-Mau,^{41,r} S. Nieswand,⁹ R. Niet,¹⁰ N. Nikitin,³³ T. Nikodem,¹² A. Nogay,⁶⁸ D. P. O'Hanlon,⁵⁰ A. Oblakowska-Mucha,²⁸ V. Obraztsov,³⁷ S. Ogilvy,¹⁹ R. Oldeman,^{16,g} C. J. G. Onderwater,⁷¹ A. Ossowska,²⁷ J. M. Otalora Goicochea,² P. Owen,⁴² A. Oyanguren,⁷⁰ P. R. Pais,⁴¹ A. Palano,^{14,l} M. Palutan,^{19,40} A. Papanestis,⁵¹ M. Pappagallo,^{14,l} L. L. Pappalardo,^{17,a} W. Parker,⁶⁰ C. Parkes,⁵⁶ G. Passaleva,¹⁸ A. Pastore,^{14,l} M. Patel,⁵⁵ C. Patrignani,^{15,h} A. Pearce,⁴⁰ A. Pellegrino,⁴³ G. Penso,²⁶ M. Pepe Altarelli,⁴⁰ S. Perazzini,⁴⁰ P. Perret,⁵ L. Pescatore,⁴¹ K. Petridis,⁴⁸ A. Petrolini,^{20,j} A. Petrov,⁶⁸ M. Petruzzo,^{22,m} E. Picatoste Olloqui,³⁸ B. Pietrzyk,⁴ M. Pikies,²⁷ D. Pinci,²⁶ A. Pistone,^{20,j} A. Piucci,¹² V. Placinta,³⁰ S. Playfer,⁵² M. Plo Casasus,³⁹ F. Polci,⁸ M. Poli Lener,¹⁹ A. Poluektov,^{50,36} I. Polyakov,⁶¹ E. Polycarpo,² G. J. Pomery,⁴⁸ S. Ponce,⁴⁰ A. Popov,³⁷ D. Popov,^{11,40} S. Poslavskii,³⁷ C. Potterat,² E. Price,⁴⁸ J. Prisciandaro,³⁹ C. Prouve,⁴⁸ V. Pugatch,⁴⁶ A. Puig Navarro,⁴² H. Pullen,⁵⁷ G. Punzi,^{24,s} W. Qian,⁵⁰ R. Quagliani,^{7,48} B. Quintana,⁵ B. Rachwal,²⁸ J. H. Rademacker,⁴⁸ M. Rama,²⁴ M. Ramos Pernas,³⁹ M. S. Rangel,² I. Raniuk,⁴⁵ F. Ratnikov,³⁵ G. Raven,⁴⁴ M. Ravonel Salzgeber,⁴⁰ M. Reboud,⁴ F. Redi,⁵⁵ S. Reichert,¹⁰ A. C. dos Reis,¹ C. Remon Alepuz,⁷⁰ V. Renaudin,⁷ S. Ricciardi,⁵¹ S. Richards,⁴⁸ M. Rihl,⁴⁰ K. Rinnert,⁵⁴ V. Rives Molina,³⁸ P. Robbe,⁷ A. Robert,⁸ A. B. Rodrigues,¹ E. Rodrigues,⁵⁹ J. A. Rodriguez Lopez,⁶⁶ P. Rodriguez Perez,⁵⁶ A. Rogozhnikov,³⁵ S. Roiser,⁴⁰ A. Rollings,⁵⁷ V. Romanovskiy,³⁷ A. Romero Vidal,³⁹ J. W. Ronayne,¹³ M. Rotondo,¹⁹ M. S. Rudolph,⁶¹ T. Ruf,⁴⁰ P. Ruiz Valls,⁷⁰ J. Ruiz Vidal,⁷⁰ J. J. Saborido Silva,³⁹ E. Sadykhov,³² N. Sagidova,³¹ B. Saitta,^{16,g} V. Salustino Guimaraes,¹ C. Sanchez Mayordomo,⁷⁰ B. Sanmartin Sedes,³⁹ R. Santacesaria,²⁶ C. Santamarina Rios,³⁹ M. Santimaria,¹⁹ E. Santovetti,^{25,i} G. Sarpis,⁵⁶ A. Sarti,²⁶

- C. Satriano,^{26,t} A. Satta,²⁵ D. M. Saunders,⁴⁸ D. Savrina,^{32,33} S. Schael,⁹ M. Schellenberg,¹⁰ M. Schiller,⁵³ H. Schindler,⁴⁰ M. Schlupp,¹⁰ M. Schmelling,¹¹ T. Schmelzer,¹⁰ B. Schmidt,⁴⁰ O. Schneider,⁴¹ A. Schopper,⁴⁰ H. F. Schreiner,⁵⁹ K. Schubert,¹⁰ M. Schubiger,⁴¹ M.-H. Schune,⁷ R. Schwemmer,⁴⁰ B. Sciascia,¹⁹ A. Sciubba,^{26,u} A. Semennikov,³² E. S. Sepulveda,⁸ A. Sergi,⁴⁷ N. Serra,⁴² J. Serrano,⁶ L. Sestini,²³ P. Seyfert,⁴⁰ M. Shapkin,³⁷ I. Shapoval,⁴⁵ Y. Shcheglov,³¹ T. Shears,⁵⁴ L. Shekhtman,^{36,f} V. Shevchenko,⁶⁸ B. G. Siddi,^{17,40} R. Silva Coutinho,⁴² L. Silva de Oliveira,² G. Simi,^{23,p} S. Simone,^{14,l} M. Sirendi,⁴⁹ N. Skidmore,⁴⁸ T. Skwarnicki,⁶¹ E. Smith,⁵⁵ I. T. Smith,⁵² J. Smith,⁴⁹ M. Smith,⁵⁵ I. Soares Lavra,¹ M. D. Sokoloff,⁵⁹ F. J. P. Soler,⁵³ B. Souza De Paula,² B. Spaan,¹⁰ P. Spradlin,⁵³ S. Sridharan,⁴⁰ F. Stagni,⁴⁰ M. Stahl,¹² S. Stahl,⁴⁰ P. Steffko,⁴¹ S. Stefkova,⁵⁵ O. Steinkamp,⁴² S. Stemmler,¹² O. Stenyakin,³⁷ M. Stepanova,³¹ H. Stevens,¹⁰ S. Stone,⁶¹ B. Storaci,⁴² S. Stracka,^{24,s} M. E. Stramaglia,⁴¹ M. Stratificiuc,³⁰ U. Straumann,⁴² J. Sun,³ L. Sun,⁶⁴ W. Sutcliffe,⁵⁵ K. Swientek,²⁸ V. Syropoulos,⁴⁴ M. Szczekowski,²⁹ T. Szumlak,²⁸ M. Szymanski,⁶³ S. T'Jampens,⁴ A. Tayduganov,⁶ T. Tekampe,¹⁰ G. Tellarini,^{17,a} F. Teubert,⁴⁰ E. Thomas,⁴⁰ J. van Tilburg,⁴³ M. J. Tilley,⁵⁵ V. Tisserand,⁴ M. Tobin,⁴¹ S. Tolk,⁴⁹ L. Tomassetti,^{17,a} D. Tonelli,²⁴ F. Toriello,⁶¹ R. Tourinho Jadallah Aoude,¹ E. Tournefier,⁴ M. Traill,⁵³ M. T. Tran,⁴¹ M. Tresch,⁴² A. Trisovic,⁴⁰ A. Tsaregorodtsev,⁶ P. Tsopelas,⁴³ A. Tully,⁴⁹ N. Tuning,^{43,40} A. Ukleja,²⁹ A. Usachov,⁷ A. Ustyuzhanin,³⁵ U. Uwer,¹² C. Vacca,^{16,g} A. Vagner,⁶⁹ V. Vagnoni,^{15,40} A. Valassi,⁴⁰ S. Valat,⁴⁰ G. Valenti,¹⁵ R. Vazquez Gomez,¹⁹ P. Vazquez Regueiro,³⁹ S. Vecchi,¹⁷ M. van Veghel,⁴³ J. J. Velthuis,⁴⁸ M. Veltri,^{18,v} G. Veneziano,⁵⁷ A. Venkateswaran,⁶¹ T. A. Verlage,⁹ M. Vernet,⁵⁷ J. V. Viana Barbosa,⁴⁰ B. Viaud,⁷ D. Vieira,⁶³ M. Vieites Diaz,³⁹ H. Viemann,⁶⁷ X. Vilasis-Cardona,^{38,b} M. Vitti,⁴⁹ V. Volkov,³³ A. Vollhardt,⁴² B. Voneki,⁴⁰ A. Vorobyev,³¹ V. Vorobyev,^{36,f} C. Voß,⁹ J. A. de Vries,⁴³ C. Vázquez Sierra,³⁹ R. Waldi,⁶⁷ C. Wallace,⁵⁰ R. Wallace,¹³ J. Walsh,²⁴ J. Wang,⁶¹ D. R. Ward,⁴⁹ H. M. Wark,⁵⁴ N. K. Watson,⁴⁷ D. Websdale,⁵⁵ A. Weiden,⁴² M. Whitehead,⁴⁰ J. Wicht,⁵⁰ G. Wilkinson,^{57,40} M. Wilkinson,⁶¹ M. Williams,⁵⁶ M. P. Williams,⁴⁷ M. Williams,⁵⁸ T. Williams,⁴⁷ F. F. Wilson,⁵¹ J. Wimberley,⁶⁰ M. Winn,⁷ J. Wishahi,¹⁰ W. Wislicki,²⁹ M. Witek,²⁷ G. Wormser,⁷ S. A. Wotton,⁴⁹ K. Wraight,⁵³ K. Wyllie,⁴⁰ Y. Xie,⁶⁵ Z. Xu,⁴ Z. Yang,³ Z. Yang,⁶⁰ Y. Yao,⁶¹ H. Yin,⁶⁵ J. Yu,⁶⁵ X. Yuan,⁶¹ O. Yushchenko,³⁷ K. A. Zarebski,⁴⁷ M. Zavertyaev,^{11,w} L. Zhang,³ Y. Zhang,⁷ A. Zhelezov,¹² Y. Zheng,⁶³ X. Zhu,³ V. Zhukov,³³ J. B. Zonneveld,⁵² and S. Zucchelli¹⁵

(LHCb Collaboration)

¹*Centro Brasileiro de Pesquisas Físicas (CBPF), Rio de Janeiro, Brazil*²*Universidade Federal do Rio de Janeiro (UFRJ), Rio de Janeiro, Brazil*³*Center for High Energy Physics, Tsinghua University, Beijing, China*⁴*LAPP, Université Savoie Mont-Blanc, CNRS/IN2P3, Annecy-Le-Vieux, France*⁵*Clermont Université, Université Blaise Pascal, CNRS/IN2P3, LPC, Clermont-Ferrand, France*⁶*Aix Marseille Univ, CNRS/IN2P3, CPPM, Marseille, France*⁷*LAL, Université Paris-Sud, CNRS/IN2P3, Orsay, France*⁸*LPNHE, Université Pierre et Marie Curie, Université Paris Diderot, CNRS/IN2P3, Paris, France*⁹*I. Physikalisches Institut, RWTH Aachen University, Aachen, Germany*¹⁰*Fakultät Physik, Technische Universität Dortmund, Dortmund, Germany*¹¹*Max-Planck-Institut für Kernphysik (MPIK), Heidelberg, Germany*¹²*Physikalisches Institut, Ruprecht-Karls-Universität Heidelberg, Heidelberg, Germany*¹³*School of Physics, University College Dublin, Dublin, Ireland*¹⁴*Sezione INFN di Bari, Bari, Italy*¹⁵*Sezione INFN di Bologna, Bologna, Italy*¹⁶*Sezione INFN di Cagliari, Cagliari, Italy*¹⁷*Università e INFN, Ferrara, Ferrara, Italy*¹⁸*Sezione INFN di Firenze, Firenze, Italy*¹⁹*Laboratori Nazionali dell'INFN di Frascati, Frascati, Italy*²⁰*Sezione INFN di Genova, Genova, Italy*²¹*Università e INFN, Milano-Bicocca, Milano, Italy*²²*Sezione di Milano, Milano, Italy*²³*Sezione INFN di Padova, Padova, Italy*²⁴*Sezione INFN di Pisa, Pisa, Italy*²⁵*Sezione INFN di Roma Tor Vergata, Roma, Italy*²⁶*Sezione INFN di Roma La Sapienza, Roma, Italy*²⁷*Henryk Niewodniczanski Institute of Nuclear Physics Polish Academy of Sciences, Kraków, Poland*

²⁸AGH—University of Science and Technology, Faculty of Physics and Applied Computer Science, Kraków, Poland²⁹National Center for Nuclear Research (NCBJ), Warsaw, Poland³⁰Horia Hulubei National Institute of Physics and Nuclear Engineering, Bucharest-Magurele, Romania³¹Petersburg Nuclear Physics Institute (PNPI), Gatchina, Russia³²Institute of Theoretical and Experimental Physics (ITEP), Moscow, Russia³³Institute of Nuclear Physics, Moscow State University (SINP MSU), Moscow, Russia³⁴Institute for Nuclear Research of the Russian Academy of Sciences (INR RAN), Moscow, Russia³⁵Yandex School of Data Analysis, Moscow, Russia³⁶Budker Institute of Nuclear Physics (SB RAS), Novosibirsk, Russia³⁷Institute for High Energy Physics (IHEP), Protvino, Russia³⁸ICCUB, Universitat de Barcelona, Barcelona, Spain³⁹Universidad de Santiago de Compostela, Santiago de Compostela, Spain⁴⁰European Organization for Nuclear Research (CERN), Geneva, Switzerland⁴¹Institute of Physics, Ecole Polytechnique Fédérale de Lausanne (EPFL), Lausanne, Switzerland⁴²Physik-Institut, Universität Zürich, Zürich, Switzerland⁴³Nikhef National Institute for Subatomic Physics, Amsterdam, The Netherlands⁴⁴Nikhef National Institute for Subatomic Physics and VU University Amsterdam, Amsterdam, The Netherlands⁴⁵NSC Kharkiv Institute of Physics and Technology (NSC KIPT), Kharkiv, Ukraine⁴⁶Institute for Nuclear Research of the National Academy of Sciences (KINR), Kyiv, Ukraine⁴⁷University of Birmingham, Birmingham, United Kingdom⁴⁸H.H. Wills Physics Laboratory, University of Bristol, Bristol, United Kingdom⁴⁹Cavendish Laboratory, University of Cambridge, Cambridge, United Kingdom⁵⁰Department of Physics, University of Warwick, Coventry, United Kingdom⁵¹STFC Rutherford Appleton Laboratory, Didcot, United Kingdom⁵²School of Physics and Astronomy, University of Edinburgh, Edinburgh, United Kingdom⁵³School of Physics and Astronomy, University of Glasgow, Glasgow, United Kingdom⁵⁴Oliver Lodge Laboratory, University of Liverpool, Liverpool, United Kingdom⁵⁵Imperial College London, London, United Kingdom⁵⁶School of Physics and Astronomy, University of Manchester, Manchester, United Kingdom⁵⁷Department of Physics, University of Oxford, Oxford, United Kingdom⁵⁸Massachusetts Institute of Technology, Cambridge, Massachusetts, USA⁵⁹University of Cincinnati, Cincinnati, Ohio, USA⁶⁰University of Maryland, College Park, Maryland, USA⁶¹Syracuse University, Syracuse, New York, USA⁶²Pontifícia Universidade Católica do Rio de Janeiro (PUC-Rio), Rio de Janeiro, Brazil

(associated with Institution Universidade Federal do Rio de Janeiro (UFRJ), Rio de Janeiro, Brazil)

⁶³University of Chinese Academy of Sciences, Beijing, China

(associated with Institution Center for High Energy Physics, Tsinghua University, Beijing, China)

⁶⁴School of Physics and Technology, Wuhan University, Wuhan, China

(associated with Institution Center for High Energy Physics, Tsinghua University, Beijing, China)

⁶⁵Institute of Particle Physics, Central China Normal University, Wuhan, Hubei, China

(associated with Institution Center for High Energy Physics, Tsinghua University, Beijing, China)

⁶⁶Departamento de Física, Universidad Nacional de Colombia, Bogota, Colombia

(associated with Institution LPNHE, Université Pierre et Marie Curie, Université Paris Diderot, CNRS/IN2P3, Paris, France)

⁶⁷Institut für Physik, Universität Rostock, Rostock, Germany

(associated with Institution Physikalisches Institut, Ruprecht-Karls-Universität Heidelberg, Heidelberg, Germany)

⁶⁸National Research Centre Kurchatov Institute, Moscow, Russia

(associated with Institution Institute of Theoretical and Experimental Physics (ITEP), Moscow, Russia)

⁶⁹National Research Tomsk Polytechnic University, Tomsk, Russia

(associated with Institution Institute of Theoretical and Experimental Physics (ITEP), Moscow, Russia)

⁷⁰Instituto de Física Corpuscular, Centro Mixto Universidad de Valencia—CSIC, Valencia, Spain

(associated with Institution ICCUB, Universitat de Barcelona, Barcelona, Spain)

⁷¹Van Swinderen Institute, University of Groningen, Groningen, The Netherlands

(associated with Institution Nikhef National Institute for Subatomic Physics, Amsterdam, The Netherlands)

[†]Deceased^aAlso at Università di Ferrara, Ferrara, Italy.^bAlso at LIFAELS, La Salle, Universitat Ramon Llull, Barcelona, Spain.^cAlso at Laboratoire Leprince-Ringuet, Palaiseau, France.^dAlso at Università di Milano Bicocca, Milano, Italy.

^eAlso at Università di Modena e Reggio Emilia, Modena, Italy.

^fAlso at Novosibirsk State University, Novosibirsk, Russia.

^gAlso at Università di Cagliari, Cagliari, Italy.

^hAlso at Università di Bologna, Bologna, Italy.

ⁱAlso at Università di Roma Tor Vergata, Roma, Italy.

^jAlso at Università di Genova, Genova, Italy.

^kAlso at Scuola Normale Superiore, Pisa, Italy.

^lAlso at Università di Bari, Bari, Italy.

^mAlso at Università degli Studi di Milano, Milano, Italy.

ⁿAlso at Universidade Federal do Triângulo Mineiro (UFTM), Uberaba-MG, Brazil.

^oAlso at AGH—University of Science and Technology, Faculty of Computer Science, Electronics and Telecommunications, Kraków, Poland.

^pAlso at Università di Padova, Padova, Italy.

^qAlso at Iligan Institute of Technology (IIT), Iligan, Philippines.

^rAlso at Hanoi University of Science, Hanoi, Viet Nam.

^sAlso at Università di Pisa, Pisa, Italy.

^tAlso at Università della Basilicata, Potenza, Italy.

^uAlso at Università di Roma La Sapienza, Roma, Italy.

^vAlso at Università di Urbino, Urbino, Italy.

^wAlso at P.N. Lebedev Physical Institute, Russian Academy of Science (LPI RAS), Moscow, Russia.